Desalination and Water Treatment
www.deswater.com

doi: 10.5004/dwt.2023.29152

282 (2023) 118–126
January

Modification of sunflower seeds waste biochar by Mg and its application for Cr(VI) adsorption from wastewater

Mohammad Mehdi Malek Mohammadi, Faranak Akhlaghian*

Department of Chemical Engineering, Faculty of Engineering, University of Kurdistan, Sanandaj, Iran,
emails: akhlaghianfk@gmail.com/fr.akhlaghian@uok.ac.ir (F. Akhlaghian), m.mehdi.mm1998@gmail.com (M.M.M. Mohammadi)

Received 9 May 2022; Accepted 28 November 2022

ABSTRACT

Water containing Cr(VI) causes health effects, which makes their treatment necessary. In this work, biochar from sunflower seeds waste was used to remove Cr(VI) from water. The biochar was modified by magnesium and optimized. The Mg-biochar was characterized by Fourier-transform infrared spectroscopy, X-ray diffraction, scanning electron microscopy (SEM), atomic force microscopy, and ASAP methods. The SEM images of Mg-biochar showed magnesium oxide spherical particles with nanoflakes. The Mg-biochar specific surface area and pore volume were 67.85 m^2/g and 0.061 m^3/g, respectively. Cr(VI) adsorption decreased from 87.16% to 50.76% with an increase in pH from 2 to 10. The isotherm of the Cr(VI) adsorption by Mg-biochar followed the Langmuir model. Thermodynamic studies showed the endothermic nature of the adsorption. Kinetics of Cr(VI) adsorption by Mg-biochar was in agreement with the pseudo-second-order model and its rate constant was 2.1 g/mg·min which was large in comparison with other works showing advantage of fast removal kinetics of Mg-biochar. The Mg-biochar adsorbent had the removal of 74.5% under the operating conditions of Cr(VI) initial concentration of 10 mg/L, adsorbent dose of 15 g/L, pH of 5, and time of 15 min.

Keywords: Biochar; Mg modification; Cr(VI) adsorption; Wastewater treatment; Sunflower seeds waste

1. Introduction

Chromium from industries, such as metal electroplating, stainless steel production, preservation of wood, paint and pigment production, and leather tanning enters water resources and pollutes them. Chromium exists commonly in two oxidation states of +3 and +6 in the environment. Cr(III) is an essential nutrient but Cr(VI) is poisonous and carcinogenic [1,2]. The World Health Organization (WHO) has limited the maximum level of total chromium in water to 50 μg/L [3].

Different methods such as the photocatalytic process, coagulation and flocculation, filtration, chemical precipitation, biological treatment, ion exchange, and adsorption have been considered to remove chromium from water [4–6]. Adsorption is an efficient method to remove Cr(VI) from water due to the use of low-cost adsorbent and high removal yield [6].

Biochar is black carbon produced from the pyrolysis of carbon rich biomass in oxygen-free conditions. Biochar is an excellent adsorbent used to remove organic and inorganic pollutants from water [7–10]. In many studies, biochar and modified biochar were used to remove pollutants from water [7–12]. Mohan et al. [13] used oak bark biochar to remove Cr(VI) from water. They found that Cr(VI) removal from water by oak bark biochar with the specific surface area of 1–3 m^2/g was equaled to activated carbon with the specific surface area of 1,000 m^2/g. Agrafioti et al. [14] used sewage sludge to prepare biochar and applied it to remove Cr(VI) and As(V) from water. Their results indicated that

* Corresponding author.

pyrolysis temperature had the most significant effect on biochar production from sewage sludge. Khalil et al. [15] showed that Cr(VI) adsorption by rice husk and tea waste biochar was a fast process. Zhang et al. [16] synthesized Fe/N co doped oak wood biochar adsorbent, reporting that after adsorption, Cr(VI) was reduced and Cr(III) complexation was achieved. Liu et al. [17] used magnetic biochar of sewage sludge to adsorb Cr(VI) from water. Bu et al. [18] prepared Fe-modified biochar of coconut shell and applied it to remove Cr(VI) from water. The adsorption capability of biochar is low [19,20]. Modification of biochar by adding metals like Mg, Ca, Fe, Al, and La improves its adsorption capability to remove PO_4^{3-}, NO_3^-, Cd, Ca, and Pb [21–27]. Magnesium is the eighth most abundant element of the earth crust with low toxicity [27–29]. Mg-biochar shows good performance for PO_4^{3-} adsorption from water [23,25,30]. Different species of Cr(VI) in water are $Cr_2O_7^{2-}$, CrO_4^{2-}, and $HCrO_4^-$ depend on pH [31].

In this work, to prepare low-cost adsorbent from agricultural waste, biochar from sunflower seeds waste from an oil pressing plant was used to remove Cr(VI) from water. Biochar was modified by Mg to improve its Cr(VI) adsorption capacity. The effects of different factors, such as pH and Cr(VI) concentration of the solution, adsorbent dose, and time on Cr(VI) removal were investigated.

2. Materials and method

2.1. Materials

Sunflower seeds waste from a local oil pressing plant was used. Potassium dichromate ($K_2Cr_2O_7$, 99.9%) for preparing chromium solution, magnesium nitrate hexahydrate ($Mg(NO_3)_2(H_2O)_6$, 99%), diphenylcarbazide ($C_{13}H_{14}N_4O$, 98%), nitric acid (HNO_3, 65%), ammonia solution (NH_3, 25%), acetone (C_3H_6O, 99.8%) purchased from Merck Company were used.

2.2. Biochar preparation

Sunflower seeds waste was milled and sieved to the mesh size of 50–60 μm. Then, it was washed with deionized water, and dried at 100°C for 12 h. In the next step, the dried biomass was transferred to a ceramic crucible with cap (oxygen-limiting conditions) in the muffle furnace at an increasing rate of 2°C/s, and pyrolyzed at 550°C for 2 h. In this way biochar was produced.

The dried sunflower seeds waste was used to prepare Mg-biochar. To 100 mL of magnesium nitrate solution 20 wt.%, 13 g of dried biomass was added and mixed by a magnetic stirrer for 15 min; then, it was dried at 100°C in an oven for 12 h. In the next step, the mixture was transferred to a ceramic crucible with cap (oxygen limiting conditions) and pyrolyzed at 550°C for 2 h with the heating ramp of 2°C/s in the muffle furnace. After cooling to the room temperature, it was milled and sieved to 50–60 μm.

2.3. Characterization equipment

Fourier-transform infrared (FTIR) spectrometer Vector 22 from Bruker Company was used to identify the functional groups constituent of Mg-biochar. The X-ray diffraction (XRD) patterns were obtained by Philips PW 1730 diffractometer with Cu kα radiation (λ = 1.5406 nm). The scanning rate was 0.05°/s with 2θ in the range of 10° to 80°. A scanning electron microscope TESCAN MIRA3 at 30.0 kV was used to study the morphology of Mg-biochar surface. A BELSORP-mini II from Microtac BZL was applied to measure the surface area and porosimetry. Atomic force microscopy (AFM) images were visualized by a Veeco Icon atomic force microscope. The light absorption of the Cr(VI) solutions was measured at 540 nm using a spectrophotometer (TG 80+, PG Company), and the Cr(VI) concentration in the solutions was calculated by the Beer–Lambert law.

2.4. Adsorption experiments

The synthetic wastewater was prepared using potassium dichromate. Then, 15 g/L of Mg-biochar was added to the Cr(VI) solution with the concentration of 10 mg/L. The mixture was agitated for 15 min at a constant rate. Then, the adsorbent was separated from the solution by centrifuge. The concentration of Cr(VI) in the solution was measured by the diphenylcarbazide method. The Cr(VI) removal was calculated by Eq. (1) [32]:

$$\mathrm{Cr(VI)removal}(\%) = \frac{C_0 - C_f}{C_0} \times 100 \quad (1)$$

where C_0 and C_f are the Cr(VI) concentration of the initial and final solution, respectively.

3. Results and discussion

3.1. Adsorbent properties

Fig. 1A presents the FTIR spectra of the biochar of sunflower seeds waste and its modification by magnesium. In the biochar spectrum, FTIR bands existed at 3,454.52 cm^{-1} (stretching vibration of O–H groups), 2,924.90 cm^{-1} (stretching vibration of aliphatic C–H), 1,738.20 cm^{-1} (stretching vibration of C=O), and 1,619.29 cm^{-1} (stretching vibration of C=C of alkenes). In the FTIR spectrum of Mg-biochar, the band at 870.87 cm^{-1} was related to the stretching vibration of CO_3^{2-}, and the band at 654.40 cm^{-1} was related to the Mg–O bound. In the FTIR spectrum of Mg-biochar, absorption bands were stronger due to the synergetic effect of magnesium ion. Fig. 1B depicts the FTIR spectra of Mg-biochar before and after Cr(VI) adsorption. After adsorption, bands at 654.40 (Mg–O), 2929.26 (C–H), 1,626.93 (C=C), and 3,453.41 cm^{-1} (O–H) were smaller because of the effects of adsorbed chromium on the surface of Mg-biochar [33,34].

Fig. 2 presents the XRD patterns of biochar and Mg-biochar before and after adsorption. In the XRD pattern of biochar, peaks at 25.1° and 27.9° were observed, which were related to the inorganic compounds in the structure of biochar [35,36]. In the XRD pattern of Mg-biochar before adsorption, in addition to the biochar peak at 27.9°, peaks at 42.45°, 62.3°, and 78.95° were observed, indicating the existence of magnesium oxide (periclase) with cubic structure and crystallinity size of 10.06 nm (by Scherrer equation) in the composition of Mg-biochar [37–39]. To prepare XRD after adsorption, first Cr(VI) adsorption by Mg-biochar was done

(operating conditions: Cr(VI) initial concentration 10 mg/L, pH 5, adsorbent dose 15 g/L, and time 30 min). Then, the adsorbent was separated and dried at 100°C in an oven for 12 h. In the XRD pattern of the Mg-biochar after adsorption peak at 28.31° was related to biochar [35,36.]. MgO reacted with water, and thus it was converted to $Mg(OH)_2$ after adsorption. In the XRD pattern, peaks at 33.71°, 36.68°, 62.23°, 74.26° were related to $Mg(OH)_2$ with hexagonal Brucite structure (JCPDS File No. 01-079-0612) [39,40]. The $Mg(OH)_2$ crystallinity size was 22.3 nm by Scherrer equation. Peaks related to chromium were not detected due to their low concentration on the surface of the Mg-biochar.

Fig. 3 shows the scanning electron microscopy (SEM) images of biochar from sunflower seeds. Sharp edges and corners of the biochar are obvious (Fig. 3A). The biochar SEM images display irregular spherical bulges, which provided efficient sites for adsorption [41,42]. In the biochar, pores are observed, which were related to the vaporization of organic compounds. The SEM images of Mg-biochar (Fig. 4) exhibit irregular spherical particles with flakes. These nanoflakes increased the specific surface area and porosity, which providing pores for adsorption. They were magnesium oxide in the structure of biochar [43]. The SEM image in Fig. 4B shows the thickness of nanoflakes in the range of 10–20 nm. The AFM image (Fig. 5) shows rough and porous surface with the maximum height of 270 nm.

Fig. 6A depicts the nitrogen adsorption/desorption of Mg-biochar. The isotherm was type IV with hysteresis H3 which indicated the slit shaped pores of Mg-biochar [44]. Furthermore, Mg-biochar pore-size distribution was unimodal with a maximum at 1.85 nm (Fig. 6B). According to the

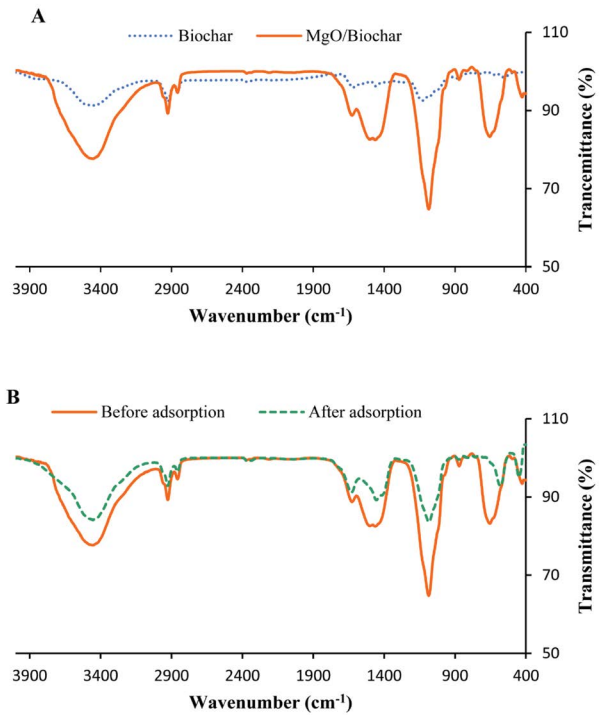

Fig. 1. FTIR spectra of (A) biochar and Mg-biochar, (B) Mg-biochar before and after Cr(VI) adsorption.

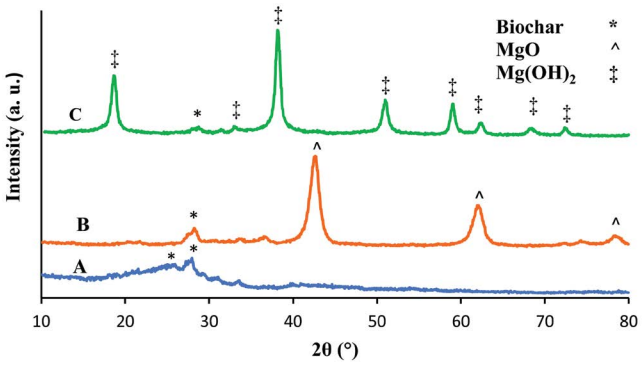

Fig. 2. XRD patterns of (A) biochar, (B) Mg-biochar before adsorption, and (C) Mg-biochar after adsorption.

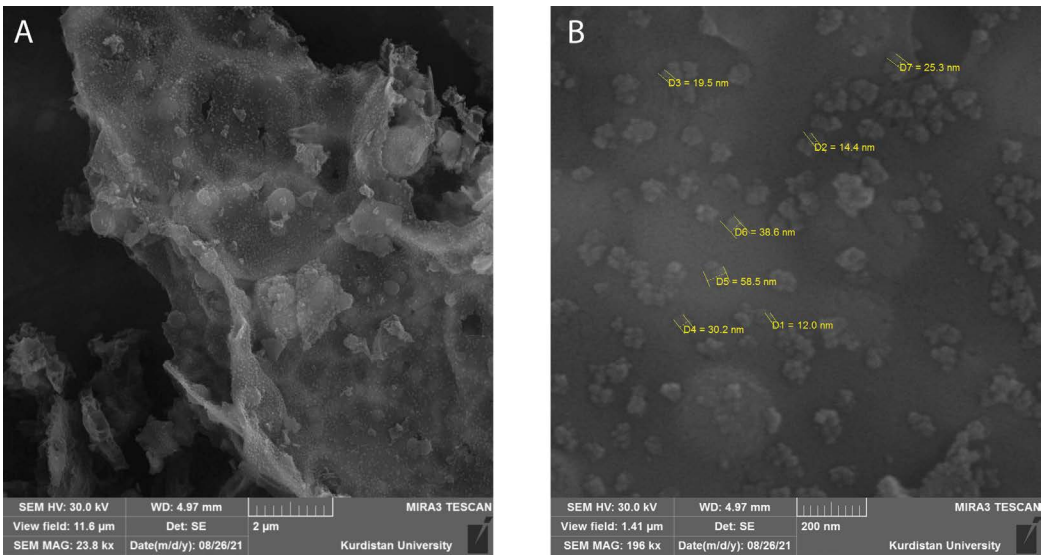

Fig. 3. SEM images of biochar.

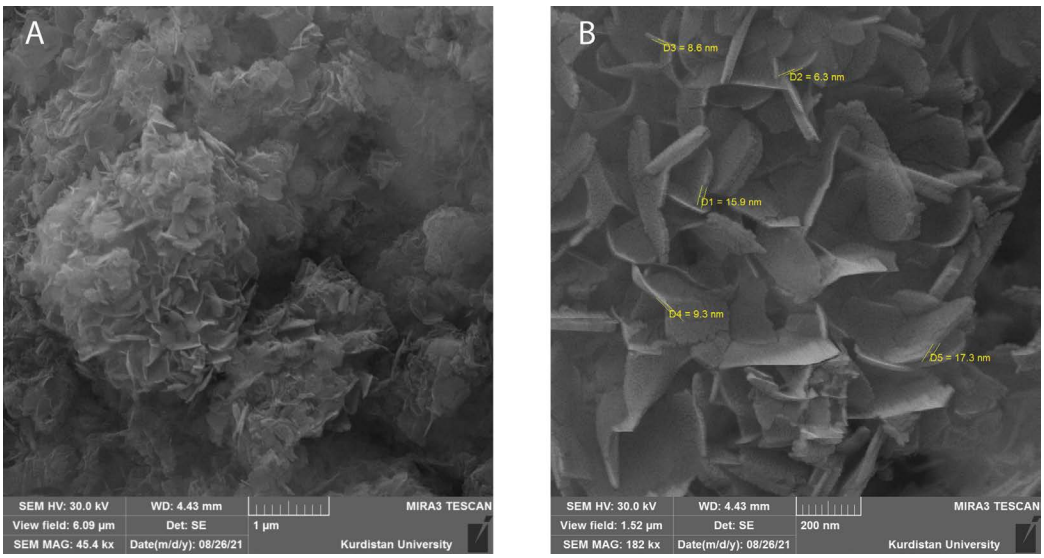

Fig. 4. SEM images of Mg-biochar.

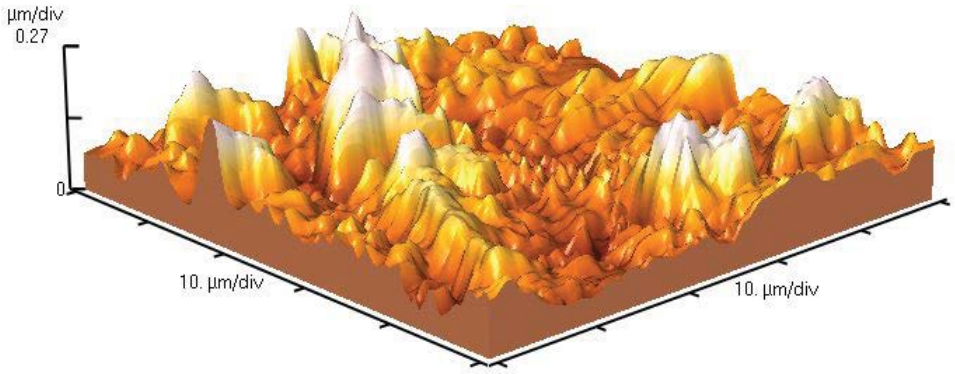

Fig. 5. AFM image of Mg-biochar.

BJH isotherm adsorption branch, the specific surface area, pore volume, and pores average diameters were 67.85 m^2/g, 0.061 m^3/g, and 1.85 nm, respectively.

3.2. Adsorbent optimization

The Mg content of the adsorbent was changed by altering the $Mg(NO_3)_2$ solution concentration in the preparation stage. Fig. 7 shows that by changing the Mg concentration of the solution from 0 to 20 wt.%, the Cr(VI) removal increased from 10% to 69%. Pure MgO was prepared by calcination $Mg(NO_3)_2$ without biochar at 550°C. In this case, the Cr(VI) removal was 33% which was lower than that of Mg-biochar, indicating the effects of biochar surface functional groups on the Cr(VI) adsorption.

The effect of the biochar pyrolysis temperature was studied (Fig. 8). The Cr(VI) removal changed from 62% to 69%, as pyrolysis temperature increased from 450°C to 550°C. However, when pyrolysis temperature increased from 550°C to 600°C, the Cr(VI) removal decreased from 69% to 60%. Hence, the pyrolysis temperature of 550°C was chosen.

3.3. Effects of the operating conditions

In this section, the effects of the operating conditions, including Cr(VI) initial concentration and pH, adsorbent dose, time, and temperature were investigated. Fig. 9A shows the effects of the Cr(VI) initial concentration in the range of 10 to 20 mg/L on adsorption. These experiments were conducted with the Mg-biochar dose of 15 g/L in the solution, pH of 5, and temperature of 25°C for 2 h. The results revealed that the Cr(VI) adsorption decreased with the increase in the Cr(VI) concentration due to an increase in the ratio of the Cr(VI) ions to adsorption actives sites [45]. Fig. 9B shows the effects of adsorbent dose in the range of 2–15 g/L in the solution with Cr(VI) concentration of 10 mg/L, pH of 5, and temperature of 25°C for 2 h. The available active sites for adsorption increased with the rise in the Mg-biochar dose; so, adsorption increased [46]. Fig. 9C displays the effects of pH in the range of 2–10 on the Cr(VI) adsorption by Mg-biochar. Dilute solutions of nitric acid and ammonia were used to adjust the pH of Cr(VI) solutions. All the experiments were conducted at Cr(VI) concentration of 10 mg/L, Mg-biochar dose of 15 g/L,

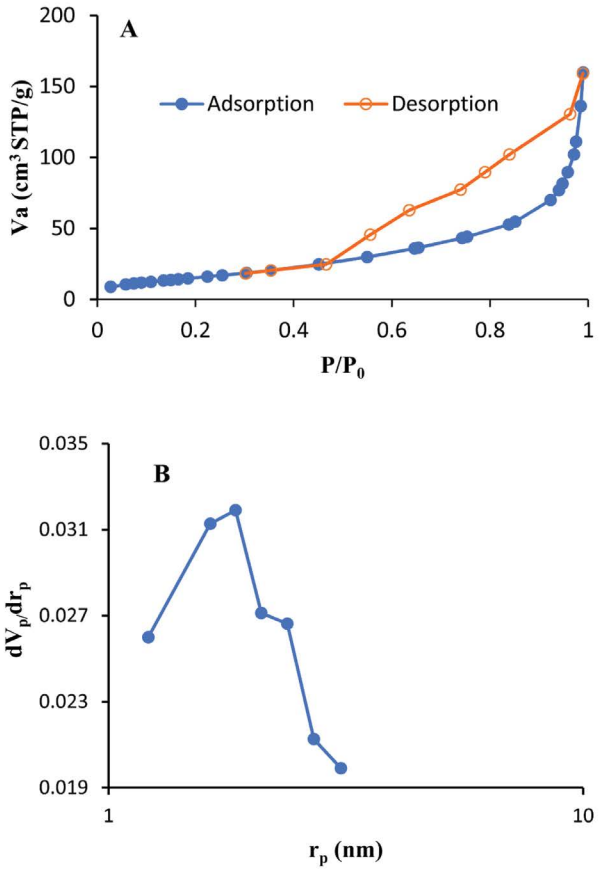

Fig. 6. Mg-biochar (A) nitrogen adsorption/desorption isotherm and (B) pore-size distribution.

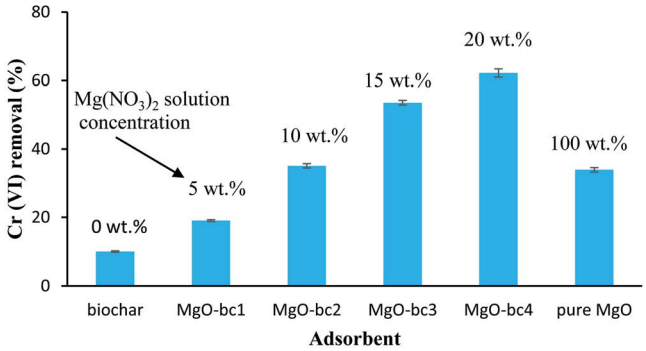

Fig. 7. Effect of the $Mg(NO_3)_2$ solution concentration of the preparation stage on the Cr(VI) adsorption.

and temperature of 25°C for 2 h. When pH increased from 2 to 10, the Cr(VI) adsorption decreased. The maximum adsorption was 88% at pH of 2. In low pH conditions, the Mg- biochar adsorbent was protonated due to the high concentration of H^+. The attractive force between positive adsorbent and negative species $Cr_3O_{10}^{2-}$, $Cr_2O_7^{2-}$, $HCrO_4^-$, $CrO_4O_{13}^{2-}$ increased the Cr(VI) adsorption. The pH of the

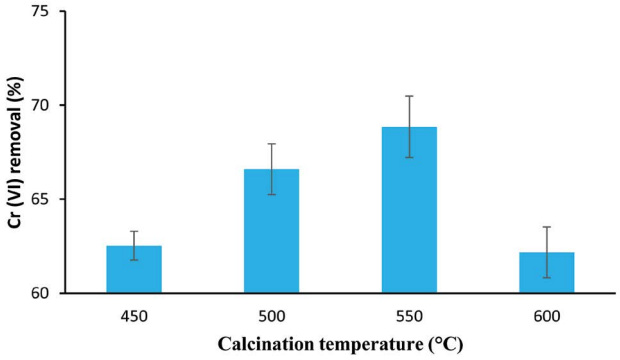

Fig. 8. Effect of pyrolysis temperature on the Cr(VI) adsorption.

zeta point was 10.30. In high pH conditions, the negative charge of Mg-biochar was reduced, and the competition between negative hydroxyl ions and negative chromium species decreased Cr(VI) adsorption [31]. Fig. 9D shows the effect of time in the range of 0–180 min on the Cr(VI) removal. In these experiments, operating conditions were Cr(VI) initial concentration of 10 mg/L, pH of 5, Mg-biochar dose of 15 g/L, and temperature of 25°C. From 0 to 15 min, the adsorption increased with time, and in durations longer than 15 min, equilibrium was reached. In other words, Cr(VI) adsorption and desorption rates were equaled; therefore, no sensible change occurred in the Cr(VI) adsorption. The effect of temperature in the range of 25°C–80°C was also investigated (Fig. 9E). These experiments were conducted at Cr(VI) concentration of 10 mg/L, adsorbent dose of 15 g/L, and pH of 5 for 2 h. Fig. 9E indicates the rise in Cr(VI) adsorption with an increase in temperature.

3.4. Kinetics, thermodynamics, and isotherm of adsorption

Pseudo-first and second-order models were used to study the kinetics of adsorption. Table 1 presents the results of fitting. The determination coefficient, R^2, of the pseudo-second-order (0.9992) was greater than the R^2 of the pseudo-first-order model (0.9737). Thus, the experimental data corresponds well to the pseudo-second-order model, and chemisorption was the rate controlling step. The large equilibrium rate constant (k_2) shows the fast kinetics of this adsorbent [46]. Fig. 9D also shows that Mg-biochar reached the equilibrium in 15 min, which compared to other adsorbents is low [31,47,48] and confirms the fast kinetics of Mg-biochar.

Eqs. (2)–(4) were used to analyze the thermodynamics of the Cr(VI) adsorption on Mg-biochar [48]:

$$\log K = \frac{\Delta S^\circ}{R} - \frac{\Delta H^\circ}{RT} \tag{2}$$

$$K = m\frac{q_e}{C_e} \tag{3}$$

$$\Delta G^\circ = \Delta H^\circ - T\Delta S^\circ \tag{4}$$

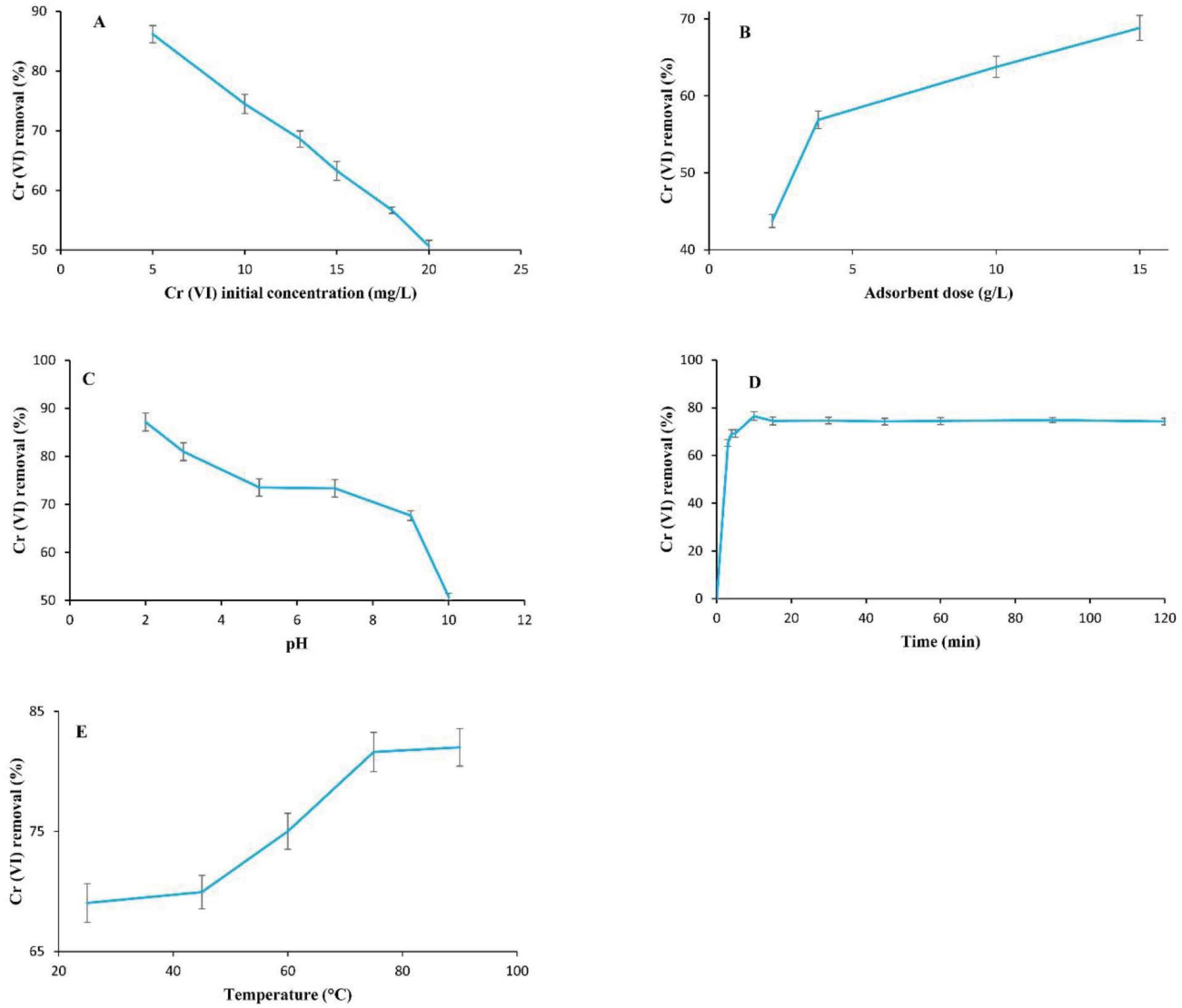

Fig. 9. Effects of operating conditions on Cr(VI) adsorption; (A) initial concentration of Cr(VI), (B) adsorbent dose, (C) pH, (D) time, and (E) temperature.

Table 1
Constants of the pseudo-first-order and pseudo-second-order kinetic models

Pseudo-first-order model	$\ln(q_{e1}-q_t)=\ln(q_{e1})-k_1t$	q_{e1} (mg/g)	0.203
		k_1 (1/min)	0.0814
		R^2	0.9737
Pseudo-second-order model	$\frac{t}{q_t}=\frac{1}{k_2q_{e2}^2}+\frac{t}{q_{e2}}$	q_{e2} (mg/g)	0.55
		k_2 (g/mg·min)	2.17
		R^2	0.9992

where R (8.314 J/mol·K) is the universal gas constant, K distribution coefficient, $\Delta S°$ entropy (J/mol), $\Delta H°$ enthalpy (J/mol·K), T temperature (K), m dose of adsorbent (g/L), q_e equilibrium adsorption capacity (mg/g), C_e equilibrium solution concentration, and $\Delta G°$ Gibbs free energy (J/mol).

The positive $\Delta H°$ shows endothermic adsorption (Table 2). Enthalpy is in the range of 0 to 20 kJ/mol, confirming the physical adsorption. According to the suggested mechanism, Cr(VI) was first converted to Cr(III), and then adsorption occurred [48]. The reaction of converting Cr(VI) to Cr(III) was endothermic. The positive $\Delta S°$ indicates an

increase in entropy and disorderness in the interface of solid and liquid. The adsorption of Cr(VI) on Mg-biochar was spontaneous due to negative Gibbs free energy.

Table 3 shows the results of fitting experimental data to Langmuir and Freundlich isotherm models. The determination coefficients of Langmuir and Freundlich models were 0.9983 and 0.9601, respectively. The greater determination coefficient and being closer to one confirmed that adsorption obeyed the Langmuir isotherm model. This model shows monolayer and homogeneous adsorption with uniform energy over the surface of Mg-biochar. The Langmuir model constants, k_l and q_m were 1.226 L/mg and 0.77 mg/g, respectively, at 25°C and pH of 5 (Table 3). Table 4 compares Mg-biochar with other adsorbents. The results showed that the maximum adsorption capacity of this work was as large as that of the others. In comparison with the others, Mg-biochar adsorption time was low and its pseudo-second-order kinetics rate constant, k_2, was large. These results confirmed that Cr(VI) adsorption by Mg-biochar is very fast which reduces adsorption process expenses. This fast adsorption kinetics is the main advantage of Mg-biochar.

Table 2
Thermodynamic analysis of the adsorption

Enthalpy (kJ/mol)	Entropy (kJ/mol·K)	Gibbs free energy (kJ/mol)				
		25°C	45°C	60°C	75°C	90°C
11.144	0.0407	–1.053	–1.866	–2.477	–3.005	–3.533

Table 3
Constants of the Langmuir and Freundlich adsorption constants

Model	Linear equation	Constants	pH = 5
Langmuir model	$\frac{C_e}{q_e}=\frac{1}{k_1 q_m}+\frac{C_e}{q_m}$	q_m (mg/g)	0.77
		k_l (L/mg)	1.226
		R^2	0.9983
Freundlich model	$\ln(q_e)=\ln(k_f)+\frac{1}{n}\ln(C_e)$	k_f ($L^{1/n}$·$mg^{1-1/n}$·g)	0.336
		n	2.56
		R^2	0.9601

3.5. Adsorption mechanism

The zeta point of Mg-biochar was 10.30. In pH lower than zeta point, the adsorbent was protonated with a positive surface charge. The electrostatic attraction between negative Cr(VI) species and positive adsorbent surface causes the Cr(VI) ions to be adsorbed by Mg-biochar. In the next stage, hydroxyl groups of adsorbent and Mg^{2+} reduced Cr(VI) to Cr(III) [53–56]. In the final stage of adsorption, the functional groups of biochar like OH participated in a coordination reaction with Cr(III) and caused Cr(III) to deposit on the adsorbent surface [53–56]. This mechanism suggested chemisorption for Cr(VI) adsorption which was in agreement with the pseudo-second-order kinetic. The schematic of the suggested mechanism of adsorption is shown in Fig. 10.

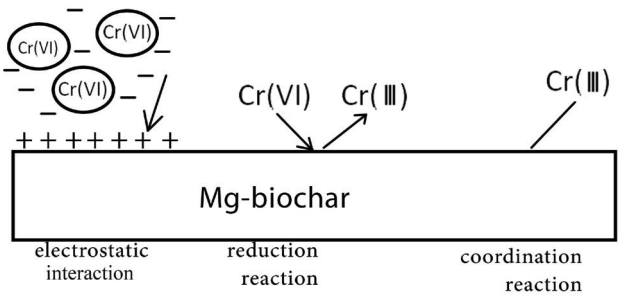

Fig. 10. Schematic of the suggested adsorption mechanism.

Table 4
Comparison with other works

Author	Adsorbent	Operating conditions	q_m (mg/g)	k_2 (g/mg·min)	References
Mohan et al. (2011)	Oak bark biochar	AD = 10 g/L, IC = 1–100 mg/L, T = 25°C, pH = 2, CT = 2,880 min	4.6	0.065	[13]
Agrafiotie et al. (2013)	Sewage sludge	AD = 4 g/L, IC = 0.2 mg/L, CT = 360 min	–	0.00017	[14]
Gorzin and Rasht Abadi (2018)	Paper mill sludge	AD = 3.5 g/L, IC = 5–300 mg/L, T = 25°C, pH = 4, CT = 240 min	30.01	0.03693	[49]
Katonta et al. (2020)	Biochar of *Phoenix reclinata* seeds	AD = 8 g/L, IC = 5–20 mg/L, T = 25°C, pH = 2, CT = 120 min	0.66	–	[48]
Zhang et al. (2020)	Carbon microsilica composite	AD = 10 g/L, IC = 1–100 mg/L, T = 25°C, pH = 2, CT = 2,880 min	18.9	0.00153	[50]
Wang et al. (2020)	Magnetically biochar of *Enteromorpha prolifera*	AD = 1 g/L, IC = 100–500 mg/L, CT = 1,440 min	86.94	0.0008	[51]
Nnadzie et al. (2020)	APTES functionalized magnetic biochar	AD = 1 g/L, IC = 10–100 mg/L, CT = 60 min	48.86	0.0127	[52]
Malek Mohammadi and Akhlaghian (2022)	Sunflower oil waste modified by Mg	AD = 15 g/L, IC = 5–20 mg/L, T = 25°C, pH = 5, CT = 15 min	0.77	2.17	This work

AD: adsorbent dose; IC: initial concentration; T: temperature; CT: contact time.

4. Conclusions

In this work, adsorption of Cr(VI) from water was studied by biochar sunflower seeds waste and its modified form by magnesium oxide. The FTIR results demonstrated that OH, C–H, C=O, C=C, and MgO functional groups were effective in Cr(VI) adsorption. In the XRD pattern of Mg-biochar, the peak at 27.95° was related to biochar inorganic compounds; and peaks at 42.95°, 62.3°, and 78.95° were related to MgO. The adsorbent was porous with slit shaped pores. The effects of operating conditions, including initial concentration, pH, adsorbent dose, time, and temperature were investigated. The experimental data were best fitted with the Langmuir isotherm model. The thermodynamic analysis revealed the endothermic and spontaneous nature of the process. The adsorption kinetics was studied which obeyed the pseudo-second-order model. The kinetics of the Cr(VI) adsorption from water by Mg-biochar was fast, which is the advantage of this adsorbent.

Acknowledgments

The authors gratefully acknowledge the financial support from the University of Kurdistan.

Conflict of interest

The authors have declared no conflict of interest.

References

[1] T. Dokmaj, T. Ibrahim, M. Khamis, M. Abouleish, I. Alam, Chemically modified nanoparticles usage for removal of chromium from sewer water, Environ. Nanotechnol. Monit. Manage., 14 (2020) 100319, doi: 10.1016/j.enmm.2020.100319.
[2] S. Pap, V. Bezanovic, J. Radonic, A. Babic, S. Saric, D. Adamovic, M.T. Sekulic, Synthesis of highly-efficient functionalized biochars from fruit industry waste biomass for the removal of chromium and lead, J. Mol. Liq., 268 (2018) 315–325.
[3] S.K. Sharma, B. Petrusevski, G. Amy, Chromium removal from water: a review, J. Water Supply Res. Technol. AQUA, 57 (2008) 541–553.
[4] H. Borji, G.M. Ayoub, R. Bilbeisi, N. Nassar, L. Malaeb, How effective are nanomaterials for the removal of heavy metals from water and wastewater?, Water Air Soil Pollut., 231 (2020) 330.
[5] Y. Yu, Q. An, L. Jin, N. Luo, Z. Li, J. Jiang, Unraveling sorption of Cr(VI) from aqueous solution by $FeCl_3$ and $ZnCl_2$-modified corn stalks biochar: implicit mechanism and application, Bioresour. Technol., 297 (2020) 122466, doi: 10.1016/j.biortech.2019.122466.
[6] M. Owlad, M.K. Aroua, W.A.W. Daud, S. Baroutian, Removal of hexavalent chromium-contaminated water and wastewater: a review, Water Air Soil Pollut., 200 (2009) 59–77.
[7] M.I. Inyang, B. Gao, Y. Yao, Y. Xue, A. Zimmerman, A. Mosa, P. Pullammanappallil, Y.S. Ok, X. Cao, A review of biochar as a low-cost adsorbent for aqueous heavy metal removal, Crit. Rev. Env. Sci. Technol., 46 (2016) 406–433.
[8] S. Elkhalifa, T. Al-Ansari, H.R. Mackey, G. McKay, Food waste to biochars through pyrolysis: a review, Resour. Conserv. Recycl., 144 (2019) 310–320.
[9] M. Waqas, A.S. Nizami, A.S. Aburiazaiza, M.A. Barakat, I.M.I. Ismail, M.I. Rashid, Optimization of food waste compost with the use of biochar, J. Environ. Manage., 216 (2018) 70–81.
[10] S. Mukherjee, A.K. Thakur, R. Goswami, P. Mazumder, K. Taki, M. Vithanage, M. Kumar, Efficacy of agricultural waste derived biochar for arsenic removal: tackling water quality in the Indo-Gangetic plain, J. Environ. Manage., 281 (2021) 111814, doi: 10.1016/j.jenvman.2020.111814.
[11] Q. Jin, Z. Wang, Y. Feng, Y.-T. Kim, A.C. Stewart, S.F. O'Keefe, A.P. Neilson, Z. He, H. Huang, Grape pomace and its secondary waste management: biochar production for a broad range of lead (Pb) removal from water, Environ. Res., 186 (2020) 109442, doi: 10.1016/j.envres.2020.109442.
[12] J. Zhang, X. Hu, J. Yan, L. Long, Y. Xue, Crayfish shell biochar modified with magnesium chloride and its effect on lead removal in aqueous solution, Environ. Sci. Pollut. Res., 27 (2020) 9582–9588.
[13] D. Mohan, S. Rajput, V. Singh, P.H. Steele, C.U. Pittman Jr., Modeling and evaluation of chromium remediation from water using low cost bio-char, a green adsorbent, J. Hazard. Mater., 188 (2011) 319–333.
[14] E. Agrafioti, G. Bouras, D. Kalderis, E. Diamadopoulos, Biochar production by sewage sludge pyrolysis, J. Anal. Appl. Pyrolysis, 101 (2013) 72–78.
[15] U. Khalil, M.B. Shakoor, S. Ali, M. Rizwan, M N. Alyemeni, L. Wijaya, Adsorption-reduction performance of tea waste and rice husk biochars for Cr(VI) elimination from wastewater, J. Saudi Chem. Soc., 24 (2020) 799–810.
[16] Y. Zhang, N. Liu, Y. Yang, J. Li, S. Wang, J. Lv, R. Tang, Novel carbothermal synthesis of Fe, N co-doped oak wood biochar (Fe/N-OB) for fast and effective Cr(VI) removal, Colloids Surf., A, 600 (2020) 124926, doi: 10.1016/j.colsurfa.2020.124926.
[17] L. Liu, X. Liu, D. Wang, H. Lin, L. Huang, Removal and reduction of Cr(VI) in simulated wastewater using magnetic biochar prepared by co-pyrolysis of nano-zero-valent iron and sewage sludge, J. Cleaner Prod., 257 (2020) 120562, doi: 10.1016/j.jclepro.2020.120562.
[18] J. Bu, W. Li, N. Niu, N. Guo, H. Zhou, C. Chen, A. Ding, Adsorption of Cr(VI) from wastewater by iron-modified coconut shell biochar, E3S Web Conf., 248 (2021) 01059, doi: 10.1051/e3sconf/202124801059.
[19] X.-J. Liu, M.-F. Li, S.K. Singh, Manganese-modified lignin biochar as adsorbent for removal of methylene blue, J. Mater. Res. Technol., 12 (2021) 1434–1445.
[20] J.Y. Qi, S. Sato, Magnesium-modified biochars for nitrate adsorption and removal in continuous flow system, Bull. Plankton Eco-Eng. Res., 1 (2021) 32–46.
[21] L.-L. Ling, W.-J. Liu, S. Zhang, H. Jiang, Magnesium oxide embedded nitrogen self-doped biochar composites: fast and high-efficiency adsorption of heavy metals in an aqueous solution, Environ. Sci. Technol., 51 (2017) 10081–10089.
[22] H. Wang, J. Dai, H. Chen, F. Wang, Y. Zhu, J. Liu, B. Zhou, R. Yuan, Adsorption of phosphate by Mg/Fe-doped wheat straw biochars optimized using response surface methodology: mechanisms and application in domestic sewage, Environ. Eng. Res., 28 (2023) 210602, doi: 10.4491/eer.2021.602.
[23] Q. Zheng, L. Yang, D. Song, S. Zhang, H. Wu, S. Li, X. Wang, High adsorption capacity of Mg–Al-modified biochar for phosphate and its potential for phosphate interception in soil, Chemosphere, 259 (2020) 127469, doi: 10.1016/j.chemosphere.2020.127469.
[24] P. Maneechakr, S. Mongkollertlop, Investigation on adsorption behaviors of heavy metal ions (Cd^{2+}, Cr^{3+}, Hg^{2+} and Pb^{2+}) through low-cost/active manganese dioxide-modified magnetic biochar derived from palm kernel cake residue, J. Environ. Chem. Eng., 8 (2020) 104467, doi: 10.1016/j.jece.2020.104467.
[25] M. Yi, Y. Chen, Enhanced phosphate adsorption on Ca-Mg-loaded biochar derived from tobacco stems, Water Sci. Technol., 78 (2018) 2427–2436.
[26] T. Liao, T. Li, X. Su, X. Yu, H. Song, Y. Zhu, Y. Zhang, $La(OH)_3$-modified magnetic pineapple biochar as novel adsorbents for efficient phosphate removal, Bioresour. Technol., 263 (2018) 207–213.
[27] Q. He, Y. Luo, Y. Feng, K. Xie, K. Zhang, S. Shen, Y. Luo, F. Wang, Biochar produced from tobacco stalks, eggshells, and Mg for phosphate adsorption from a wide range of pH aqueous solutions, Mater. Res. Express, 7 (2020) 115603, doi: 10.1088/2053-1591/abcb3d.

[28] Magnesium (Mg) and Water, 2022. Available at: https://www.lenntech.com/periodic/water/magnesium/magnesium-and-water.htm [Accessed 9/3/2022].
[29] Magnesium, 2022. Available at: https://www.canada.ca › water-magnesium-eau-eng [Accessed 9/3/2022].
[30] C. Fang, T. Zhang, P. Li, R.-F. Jiang, Y.-C. Wang, Application of magnesium modified corn biochar for phosphorus removal and recovery from swine wastewater, Int. J. Environ. Res. Public Health, 11 (2014) 9217–9237.
[31] N. Ballav, H.J. Choi, S.B. Mishra, A. Maity, Synthesis, characterization of Fe_3O_4@glycine doped polypyrrole magnetic nanocomposites and their potential performance to remove toxic Cr(VI), J. Ind. Eng., 20 (2014) 4085–4093.
[32] P. Wang, I.M.C. Lo, Synthesis of mesoporous magnetic γ-Fe_2O_3 and its application to Cr(VI) removal from contaminated water, Water Res., 43 (2009) 3727–3734.
[33] Y. Liu, Z. He, M. Uchimiya, Comparison of biochar formation from various agricultural by-products using FTIR spectroscopy, Mod. Appl. Sci., 9 (2015) 246–253.
[34] A. Li, H. Deng, Y. Jiang, C. Ye, B. Yu, X. Zhou, A. Ma, Super-efficient removal of heavy metals from wastewater by Mg-loaded biochars: adsorption characteristics and removal mechanism, Langmuir, 36 (2020) 9160–9174.
[35] A.M. Dehkhoda, N. Ellis, E. Gyenge, Electrosorption on activated biochar: effect of thermo-chemical activation treatment on the electric double layer capacitance, J. Appl. Electrochem., 44 (2014) 141–157.
[36] Y. Liu, X. Zhao, J. Li, D. Ma, R. Han, Characterization of biochar from pyrolysis of wheat straw and its evaluation on methylene blue adsorption, Desal. Water Treat., 46 (2012) 115–123.
[37] Y. Deng, X. Li, F. Ni, Q. Liu, Y. Yang, M. Wang, T. Ao, W. Chen, Synthesis of magnesium modified biochar for removing copper, lead and cadmium in single and binary systems from aqueous solutions: adsorption mechanism, Water, 13 (2021) 599, doi: 10.3390/w13050599.
[38] L. Ge, W. Wang, Z. Peng, F. Tan, X. Wang, J. Chen, X. Qiao, Facile fabrication of Fe@MgO magnetic nanocomposites for efficient removal of heavy metal ion and dye from water, Powder Technol., 326 (2018) 393–401.
[39] Y. Chen, T. Zhou, H. Fang, S. Li, Y. Yao, Y. He, A novel preparation of nano-sized hexagonal $Mg(OH)_2$, Procedia Eng., 102 (2015) 388–394.
[40] K.M. Saoud, S. Saeed, R.M. Al-Soubaihi, M.F. Bertino, Microwave assisted preparation of magnesium hydroxide nano-sheets, Am. J. Nanomater., 2 (2014) 21–25.
[41] M. Saffari, Response surface methodological approach for optimizing the removal of cadmium from aqueous solutions using pistachio residues biochar supported/non-supported by nanoscale zero-valent iron, Main Group Met. Chem., 41 (2018) 167–181.
[42] C. Yu, H. Wang, M. Lu, F. Zhu, Y. Yang, H. Huang, C. Zou, J. Xiong, Z. Zhong, Application of rice straw, corn cob, and lotus leaf as agricultural waste derived catalysts for low temperature SCR process: optimization of preparation process, catalytic activity and characterization, Aerosol Air Qual. Res., 20 (2020) 862–876.
[43] M. Zhang, B. Gao, Y. Yao, Y. Xue, M. Inyang, Synthesis of porous MgO-biochar nanocomposites for removal of phosphate and nitrate from aqueous solutions, Chem. Eng. J., 210 (2012) 26–32.
[44] G. Leofanta, M. Padovan, G. Tozzola, B. Venturelli, Surface area and pore texture of catalysts, Catal. Today, 41 (1998) 207–219.
[45] K. Ahalya, N. Suriyanarayanan, V. Ranjithkumar, Effect of cobalt substitution on structural and magnetic properties and chromium adsorption of manganese ferrite nano particles, J. Magn. Magn. Mater., 372 (2014) 208–213.
[46] S. Chen, Q. Yue, B. Gao, X. Xu, Equilibrium and kinetic adsorption study of the adsorptive removal of Cr(VI) using modified wheat residue, J. Colloid Interface Sci., 349 (2010) 256–264.
[47] N. Mehrabi, M. Soleimani, M. Madadi Yeganeh, H. Sharififard, Parameters optimization for nitrate removal from water using activated carbon and composite of activated carbon and Fe_2O_3 nanoparticles, RSC Adv., 5 (2015) 51470–51482.
[48] J. Katenta, C. Nakiguli, P. Mukasa, E. Ntambi, Removal of chromium(VI) from tannery effluent using bio-char of *Phoenix reclinata* seeds, Green Sustainable Chem., 10 (2020) 91–107.
[49] F. Gorzin, M.M. Bahri Rasht Abadi, Adsorption of Cr(VI) from aqueous solution by adsorbent prepared from paper mill sludge: kinetics and thermodynamics studies, Adsorpt. Sci. Technol., 36 (2018) 149–169.
[50] D. Zhang, Y. Ma, H. Feng, Y. Hao, Adsorption of Cr(VI) from aqueous solution using carbon-microsilica composite adsorbent, J. Chil. Chem. Soc., 57 (2012) 964–968.
[51] Y. Wang, Q. Yang, J. Chen, J. Yang, Y. Zhang, Y. Chen, X. Li, W. Du, A. Liang, S.-H. Ho, J.-S. Chang, Adsorption behavior of Cr(VI) by magnetically modified *Enteromorpha prolifera* based biochar and the toxicity analysis, J. Hazard. Mater., 395 (2020) 122658, doi: 10.1016/j.jhazmat.2020.122658.
[52] E.C. Nnadozie, P. Ajibade, Adsorption, kinetic and mechanistic studies of Pb(II) and Cr(VI) ions using APTES functionalized magnetic biochar, Microporous Mesoporous Mater., 309 (2020) 110573, doi: 10.1016/j.micromeso.2020.110573.
[53] Y. Huang, B. Wang, J. Lv, Y. He, H.H. Zhang, W. Li, Y. Li, T. Wågberg, G. Hu, Facile synthesis of sodium lignosulfonate/polyethyleneimine/sodium alginate beads with ultra-high adsorption capacity for Cr(VI) removal from water, J. Hazard. Mater., 436 (2020) 129270, doi: 10.1016/j.jhazmat.2022.129270.
[54] B. Ren, Y. Jin, L. Zhao, C. Cui, X. Song, Enhanced Cr(VI) adsorption using chemically modified dormant *Aspergillus niger* spores: process and mechanisms, J. Environ. Chem. Eng. 10 (2022) 106955, doi: 10.1016/j.jece.2021.106955.
[55] J. Begum, Z. Hussian, T. Noor, Adsorption and kinetic study of Cr(VI) on ZIF-8 based composites, Mater. Res. Express, 7 (2020) 015083, doi: 10.1088/2053-1591/ab6b66.
[56] D.R. Vaddi, T.R. Gurugubelli, R. Koutavarapu, D.-Y. Lee, J. Shim, Bio-stimulated adsorption of Cr(VI) from aqueous solution by groundnut shell activated Carbon@Al embedded material, Catalysts, 12 (2022) 290, doi: 10.3390/catal12030290.